Stability and Size-Discriminating Effects in Mononuclear Lanthanide Triple-Helical Building Blocks with Tridentate Aromatic Ligands

Stéphane Petoud,[†] Jean-Claude G. Bünzli,*[,†] Fabien Renaud,[‡] Claude Piguet,*[,‡] Kurt J. Schenk,[§] and Gérard Hopfgartner[||]

Institute of Inorganic and Analytical Chemistry, BCH, and the Institute of Crystallography, BSP, University of Lausanne, CH-1015-Lausanne, Switzerland, Department of Inorganic, Analytical and Applied Chemistry, Sciences II, University of Geneva, CH-1211 Geneva-4, Switzerland, and Pharma Division, Hoffmann-La Roche, CH-4070 Basle, Switzerland

Received June 5, 1997[⊗]

The planar aromatic tridentate ligand 2,6-bis(1-methylbenzimidazol-2-yl)pyridine (L^1) reacts with Ln^{III} (Ln = La−Lu) in acetonitrile to give the successive complexes $[Ln(L^1)_n]^{3+}$ ($n = 1-3$). Stability constants determined by spectrophotometry and potentiometric competitive titrations with Ag^I show that the 1:1 and the 1:2 complexes display the usual thermodynamic behavior associated with electrostatic effects while the 1:3 complexes exhibit an unusual selectivity for the midrange Ln^{III} ions ($\Delta \log K_3(Gd-Lu) \approx 4$). A detailed investigation of the solution structure of $[Ln(L^1)_3]^{3+}$ (Ln = La−Dy) reveals that the closely packed triple-helical structure found in the crystal structure of $[Eu(L^1)_3]^{3+}$ is retained in acetonitrile for the complete series. A sharp control of the coordination cavity results from the interstrand π-stacking interactions which appear to be optimum for Gd^{III}. For Yb^{III}, for instance, a 1:2 complex only could be isolated, which crystallizes as a hydroxo-bridged dimer $[Yb(OH)(L^1)_2]_2(ClO_4)_4(HClO_4)_{0.5}(CH_3CN)_{7.32}(L^1)_{0.5}$ (triclinic, $P\bar{1}$, $a = 13.250(2)$ Å, $b = 16.329(2)$ Å, $c = 27.653(3)$ Å, $\alpha = 99.941(9)°$, $\beta = 93.394(9)°$, $\gamma = 108.114(9)°$, $Z = 2$). The binding of bulky substituents to the nitrogen atoms of the benzimidazole side arms in L^4 (i) severely affects the wrapping process, (ii) leads to less stable triple-helical building blocks, and (iii) removes the size-discriminating effect. The last can however be restored if a strong electron-donor group is connected to the central pyridine ring in L^8. Stability and solution structure data for $[Ag_2(L^i)_2]^{2+}$ ($i = 1, 4, 8$) are also reported and discussed.

Introduction

The initial work of Weissman,[1] who demonstrated in 1942 that the metal-centered luminescence of Eu^{III} β-diketonates is sensitized by energy transfer from the ligand excited states, stirred a lot of interest in the relationship between structural and spectroscopic properties of lanthanide-containing coordination complexes. Initially, lanthanide chelates were studied for their potential use as luminescent materials in liquid lasers,[2] but the first application appeared in the field of biomedical analyses in the beginning of the 1980s with the commercial availability of time-resolved fluoroimmunoassays.[3,4] Many other biomedical applications have since emerged,[5] some relying on luminescent properties of the Ln^{III} ions, mainly Eu^{III}, Tb^{III}, and, to a lesser extent, Sm^{III}, such as probing metallic sites in proteins[6] or molecular interactions in biological media[4] and cancer phototherapy.[7] The design of lanthanide-containing luminescent stains has to overcome two difficulties arising from the particularly low oscillator strengths of the f−f transitions and from the easy deexcitation of the Ln^{III} excited states.[8−10] To master these challenges, chemists have encapsulated the Ln^{III} ions in supramolecular edifices providing fairly rigid and well-protected environments, using preorganized ligands such as coronands, cryptands,[11] calixarenes,[12,13] or Schiff bases.[14] Another design strategy includes the use of multidentate podands[15] and of self-assembly processes.[16−18] The recent development of dinuclear d−f and f−f complexes working as efficient DNA and RNA sequencing agents,[19] magnetic probes,[20] and directional light converters[21,22] requires an even closer

[†] Institute of Inorgagnic and Analytical Chemistry, University of Lausanne.
[‡] University of Geneva.
[§] Institute of Crystallography, University of Lausanne.
[||] F. Hoffman-La Roche.
[⊗] Abstract published in *Advance ACS Abstracts,* November 15, 1997.

(1) Weissman, S. I. *J. Chem. Phys.* **1942**, *10*, 214.
(2) Reisfeld, R.; Jorgensen, C. K. *Lasers and Excited States of Rare Earths*; Springer-Verlag: Berlin, 1977.
(3) Soini, E.; Loevgren, T. N. E. *CRC Crit. Rev. Anal. Chem.* **1987**, *18*, 105.
(4) Mathis, G. *Clin. Chem.* **1995**, *41*, 1391.
(5) *Lanthanide Probes in Life, Chemical and Earth Sciences: Theory and Practice*; Bünzli, J.-C. G., Choppin, G. R., Eds.; Elsevier Science: Amsterdam, 1989.
(6) Bünzli, J.-C. G.; Pfefferlé, J. M. *Helv. Chim. Acta* **1994**, *77*, 323.
(7) Sessler, J. L.; Kral, V.; Hoehner, M. C.; Chin, K. O. A.; Davila, R. M. *Pure Appl. Chem.* **1996**, *68*, 1291.
(8) Dickins, R. S.; Parker, D.; de Sousa, A. S.; Williams, J. A. G. *J. Chem. Soc., Chem. Commun.* **1996**, 697.
(9) Bünzli, J.-C. G.; Froidevaux, P.; Harrowfield, J. M. *Inorg. Chem.* **1993**, *32*, 3306.
(10) Blasse, G.; Dirksen, G. J.; Sabbatini, N.; Perathoner, S.; Lehn, J.-M.; Alpha, B. *J. Phys. Chem.* **1988**, *92*, 2419.
(11) Alexander, V. *Chem. Rev.* **1995**, *95*, 273.
(12) Bünzli, J.-C. G.; Harrowfield, J. M. In *Calixarenes: a Versatile Class of Macrocyclic Compounds*; Vicens, J., Böhmer, V., Eds.; Kluwer Academic: Dordrecht, The Netherland, 1991; pp 211−31.
(13) Bünzli, J.-C. G.; Ihringer, F. *Inorg. Chim. Acta* **1996**, *246*, 195.
(14) Guerriero, P.; Tamburini, S.; Vigato, P. A. *Coord. Chem. Rev.* **1995**, *139*, 17.
(15) Jones, P. L.; Amoroso, A. J.; Jeffery, J. C.; McCleverty, J. A.; Psillakis, E.; Rees; L. H.; Ward, M. D. *Inorg. Chem.* **1997**, *36*, 10.
(16) Piguet, C.; Bernardinelli, G.; Hopfgartner, G. *Chem. Rev.* **1997**, *97*, 2005.
(17) Latva, M.; Makinen, P.; Kulmala, S.; Haapakka, K. *J. Chem. Soc., Faraday Trans. I* **1996**, *92*, 3321.
(18) Lehn, J.-M. *Supramolecular Chemistry. Concepts and Perspectives*; VCH: Weinheim, New York, Basel, Cambridge, Tokyo, 1995.
(19) Hurst, P.; Takasaki, B. K.; Chin, J. *J. Am. Chem. Soc.* **1996**, *118*, 9982. Raganathan, K. G.; Schneider, H. J. *Angew. Chem., Int. Ed. Engl*. **1996**, *35*, 1219.
(20) Costes, J.-P.; Dahan, F.; Dupuis, A.; Laurent, J.-P. *Inorg. Chem*. **1996**, *35*, 2400. Ramade, I.; Kahn, O.; Jeanin, Y.; Robert, F. *Inorg. Chem*. **1997**, *36*, 930.
(21) Piguet, C.; Bünzli, J.-C. G.; Bernardinelli, G.; Hopfgartner, G.; Williams, A. F. *J. Am. Chem. Soc.* **1993**, *115*, 8197.

S0020-1669(97)00693-9 CCC: $14.00

Chart 1

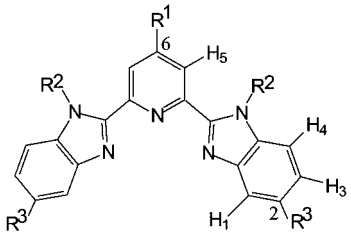

L	R^1	R^2	R^3
L^0	H	H	H
L^1	H	Me	H
L^2	H	Et	H
L^3	H	Oct	H
L^4	H	$Bz(OMe)_2$	H
L^5	H	Et	Me
L^6	Phe	$Bz(OMe)_2$	H
L^7	$PheNO_2$	$Bz(OMe)_2$	H
L^8	$PheNEt_2$	$Bz(OMe)_2$	H

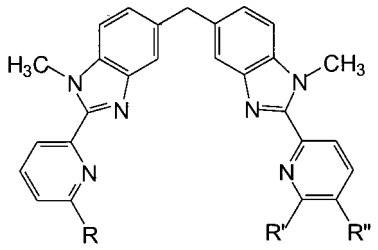

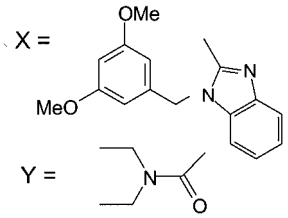

L^9	R = X, R' = H, R'' = Me
L^{10}	R = Y, R' = H, R'' = Me
L^{11}	R = R' = X, R'' = H

control and predictable tuning of the Ln^{III} coordination sphere to enhance the final properties of these devices.

In recent years, much work has been carried out in our laboratories based on self-assembly processes associated with the weak coordination requirements of the Ln^{III} ions, namely their preference for a nine-coordinated, tricapped trigonal prismatic (ttp) arrangement with idealized D_{3h} symmetry, as found in the solvates with monodentate ligands such as water or acetonitrile.[23] We have shown that a judicious design of the ligand-binding possibilities and secondary noncovalent interactions (stacking, van der Waals, etc.) leads to lanthanide complexes with predetermined structural and electronic properties. Luminescent and neutral complexes $[Ln(NO_3)_3(L^i)(solv)]$ result from the reaction of ligands L^i ($i = 1-8$; *cf.* Chart 1) with $Ln(NO_3)_3$,[24,25] while triple-helical complexes $[Ln(L^i)_3]^{3+}$ are formed with lanthanide perchlorates.[26,27] The unsymmetrical segmental ligands L^9 and L^{10} self-assemble with mixtures of Ln^{III} and M^{II} (M = Zn, Fe) ions leading to triple-stranded noncovalent heterodinuclear d−f podates $[LnM(L^i)_3]^{5+}$ where each metal ion occupies a specific coordination site.[28−33] Finally, homodinuclear f−f triple-stranded helicates $[Ln_2(L^{11})_3]^{6+}$ have been prepared upon reaction of the bis-tridentate ligand L^{11} with Ln^{III}, but the selective synthesis of pure heterodinuclear f−f complexes remains a challenge.[21,34] One of our aims is to design unsymmetrical ligands similar to L^{11} but bearing different substituents bound to the tridentate units which predispose[35] them to recognize and complex selectively two Ln^{III} ions having different ionic radii. Such supramolecular edifices would be ideal model molecules for testing the mechanism of lanthanide-to-lanthanide energy transfer processes. They would also provide two probes in one luminescent stain and present potentialities in the field of luminescence imaging of biological material. This approach requires a deep understanding of the structural and electronic factors which control the wrapping of the strands in order to design Ln^{III} coordination spheres with predictable sizes in the final self-assembled architectures. As a step toward this goal, we investigate here (i) the effect of substituents R^1 and R^2 (L^1, L^4, L^7, L^8) on the thermodynamic stability of the mononuclear triple-helical complexes $[Ln(L^i)_3]^{3+}$ and on the associated size-discriminating effect, (ii) the stabilization of the +3 oxidation state relative to the +2 state in $[Eu(L^1)_3]^{n+}$, and (iii) the solution structure of $[Ln(L^1)_3]^{3+}$.

Experimental Section

Solvents and starting materials were purchased from Fluka AG (Buchs, Switzerland) and used without further purification unless otherwise stated. Acetonitrile was distilled from CaH_2 and P_2O_5. Dichloromethane (CH_2Cl_2), *N*,*N*-dimethylformamide (DMF), and triethylamine were distilled from CaH_2. Lanthanide perchlorates and trifluoromethanesulfonates (triflates) were prepared from the oxides (Glucydur, 99.99%) and dried according to published procedures.[36,37] The Ln content of solutions and solid salts was determined by complexometric titrations with Titriplex III (Merck) in the presence of urotropine and xylene orange.[38] The Ag content of solutions was determined by potentiometric titrations with KCl (working electrode Ag; reference electrode $Hg/Hg_2SO_4/K_2SO_4$). Analytical grade $AgClO_4$ (Fluka) was dried under vacuum (10^{-2} Torr; 14 h at 40 °C and 48 h at 60−70 °C). NEt_4ClO_4 (Fluka, purum) was purified according to Almasio et al.[39] and dried for 24 h in a desiccator containing KOH and for 72 h under vacuum (10^{-2} Torr, 40 °C). ***Caution!*** Dry perchlorates may explode and should be handled in small quantities and with the necessary precautions.

(22) Matthews, K. D.; Bailey-Folkes, S. A.; Kahwa, I. A.; McPherson, G. L.; O'Mahoney, C. A.; Ley, S. V.; Williams, D. J.; Groombridge, C. J.; O'Connor, C. A. *J. Phys. Chem.* **1992**, *96*, 7021.
(23) Moret, E.; Nicolo, F.; Bünzli, J.-C. G.; Chapuis, G. *J. Less-Common Met.* **1991**, *171*, 273.
(24) Piguet, C.; Williams, A. F.; Bernardinelli, G.; Moret, E.; Bünzli, J.-C. G. *Helv. Chim. Acta* **1992**, *75*, 1697.
(25) Petoud, S.; Bünzli, J.-C. G.; Schenk, K. J.; Piguet, C. *Inorg. Chem.* **1997**, *36*, 1345.
(26) Piguet, C.; Bünzli, J.-C. G.; Bernardinelli, G.; Bochet, C. G.; Froidevaux, P. *J. Chem. Soc., Dalton Trans.* **1995**, 83.
(27) Piguet, C.; Williams, A. F.; Bernardinelli, G.; Bünzli, J.-C. G. *Inorg. Chem.* **1993**, *32*, 4139.
(28) Piguet, C.; Rivara-Minten, E.; Bernardinelli, G.; Bünzli, J.-C. G.; Hopfgartner, G. *J. Chem. Soc., Dalton Trans.* **1997**, 421.
(29) Piguet, C.; Bünzli, J.-C. G.; Bernardinelli, G.; Hopfgartner, G.; Petoud, S.; Schaad, O. *J. Am. Chem. Soc.* **1996**, *118*, 6681.
(30) Piguet, C.; Hopfgartner, G.; Williams, A. F.; Bünzli, J.-C. G. *J. Chem. Soc., Chem. Commun.* **1995**, 491.
(31) Piguet, C.; Rivara-Minten, E.; Hopfgartner, G.; Bünzli, J.-C. G. *Helv. Chim. Acta* **1995**, *78*, 1541.
(32) Piguet, C.; Bernardinelli, G.; Bünzli, J.-C. G.; Petoud, S.; Hopfgartner, G. *J. Chem. Soc., Chem. Commun.* **1995**, 2575.
(33) Piguet, C.; Rivara-Minten, E.; Hopfgartner, G.; Bünzli, J.-C. G. *Helv. Chim. Acta* **1995**, *78*, 1651.
(34) Bernardinelli, G.; Piguet, C.; Williams, A. F. *Angew. Chem., Int. Ed. Engl.* **1992**, *31*, 1622.
(35) Rowan, S. J.; Hamilton, D. G.; Brady, P. A.; Sanders, J. K. M. *J. Am. Chem. Soc.* **1997**, *119*, 2578.
(36) Bünzli, J.-C. G.; Mabillard, C. *Inorg. Chem.* **1986**, *25*, 2750.
(37) Bünzli, J.-C. G.; Pilloud, F. *Inorg. Chem.* **1989**, *28*, 2638.
(38) Schwarzenbach, G. *Die komplexometrische Titration*; F. Enke: Stuttgart, Germany, 1957.
(39) Almasio, M.-C.; Arnaud-Neu, F.; Schwing-Weill, M.-J. *Helv. Chim. Acta* **1983**, *66*, 1296.

Preparation of the Ligands and Complexes. Ligands L^1, L^4, L^7, and L^8 were synthesized according to procedures previously described.[26,40] Systematic nomenclature is as follows. 2,6-Bis(1-X-benzimidazol-2-yl)pyridine: X = methyl, L^1; X = 3,5-dimethoxybenzyl, L^4. 2,6-Bis[1-(3,5-dimethoxybenzyl)benzimidazol-2-yl)]-4-X-pyridine: X = 4-nitrophenyl, L^7; X = 4-(diethylamino)phenyl, L^8. Complexes were isolated by following the procedure previously reported.[26]

Preparation of $[Yb(OH)(L^1)_2]_2(ClO_4)_4(HClO_4)_{0.5}(CH_3CN)_{7.32}(L^1)_{0.5}$ (1). Single crystals of **1** were obtained while attempts were made to crystallize the 1:3 complex. A solution of 40.03 mg of L^1 (0.118 mmol, 3 equiv) in 540 μL of CH_2Cl_2 was added dropwise under vigorous stirring to 23.07 mg of $Yb(ClO_4)_3 \cdot 6.3H_2O$ (0.039 mmol) in 700 μL of MeCN. A yellow coloration appeared immediately, and the solution was stirred for 1 h, the solvents were removed, and the solid residue was dried for 2 h (10^{-2} Torr, 40 °C). The complex was dissolved in 1.5 mL of MeCN at 30 °C and under ultrasonic irradiation. The resulting solution was filtered, and the solution was left at room temperature. Yellow single crystals suitable for X-ray analysis appeared after several weeks.

Preparation and Characterization of $[Ag_2(L^i)_2](ClO_4)_2$ (i = 1, 4, and 8). A solution of 166 mg of $AgClO_4 \cdot H_2O$ (0.737 mmol) in 10 mL of MeCN was added dropwise under stirring to 250 mg of L^1 (0.737 mmol) in 30 mL of CH_2Cl_2/MeCN, 2:1 v/v. The solution was stirred in the dark for 2 h at room temperature and the solvents were removed. The white solid was recrystallized in 50 mL of MeCN, and the fine needles were dried for 2 h (10^{-2} Torr, 40 °C). Yield: 620 mg (76%). Anal. Calcd for $[Ag_2(L^1)_2](ClO_4)_2 \cdot H_2O$, $Ag_2C_{42}H_{36}N_{10}Cl_2O_9$ (fw 1111.46): Ag, 19.41; C, 45.39; H, 3.08; N, 12.60. Found: Ag, 19.40; C, 45.61; H, 3.13; N, 12.57. IR (KBr, cm^{-1}): 3100, 3060 (w, ν_{CH}(arom)); 2940 (w, ν_{CH}(aliph)); 1595, 1570 (m), 1475 (s, $\nu_{C=C}$, $\nu_{C=N}$); 1420, 1405 (s, $\nu_{C=C}$, $\nu_{C=N}$, $\delta_{as\ CH_3}$); 1380 (w, $\delta_{s\ CH_3}$); 1090 (vs, ν_{ClO_4}); 750 (s, $\delta_{CH\ arom}$); 625 (s, δ_{ClO_4}). ^{1}H-NMR (200 MHz, CD_3NO_2, ppm with reference to TMS): 3.93 (s, 6H), 7.1−7.4 (m, 8H), 8.38 (d, 2H, ^3J = 7.5 Hz), 8.35 (t, 2H, ^3J = 7.5 Hz). UV−vis (propylene carbonate, cm^{-1}): 30 960 (ϵ = 46 100 M^{-1} cm^{-1}), 32 787 (46 740). ES-MS (CH_3CN): m/z 446.9 $[Ag_2(L^1)_2]^{2+}$.

A solution of 73.6 mg of $Ag(ClO_4) \cdot H_2O$ (0.33 mmol) in 10 mL of MeCN was added dropwise under stirring to 200 mg of L^4 (0.33 mmol) in 30 mL of CH_2Cl_2/MeCN, 2:1 v/v. The solution was stirred in the dark for 2 h at room temperature, and the solvents were removed. The white solid was redissolved in 12 mL of MeCN, and diethyl ether was diffused through the solution for 12 h. The fine needles were filtered off and dried for 2 h (10^{-2} Torr, 40 °C). Yield: 225 mg (81%). Anal. Calcd for $[Ag_2(L^4)_2](ClO_4)_2 \cdot 3H_2O$, $Ag_2C_{74}H_{72}N_{10}O_{19}Cl_2$ (fw 1692.10): Ag, 12.75; C, 52.53; H, 4.29; N, 8.28. Found: Ag, 12.63; C, 52.63; H, 4.35; N, 8.28. IR (KBr, cm^{-1}): 3100, 3080 (w, $\nu_{CH\ arom}$); 2940, 2840 (w, $\nu_{CH\ aliph}$); 1595 (vs), 1515 (m), 1462 (vs, $\nu_{C=C}$, $\nu_{C=N}$); 1420 (s, $\nu_{C=C}$, $\nu_{C=N}$, $\delta_{as\ CH_3}$); 1381 (m, $\delta_{s\ CH_3}$); 1089 (vs, ν_{ClO_4}); 750 (s, $\delta_{CH\ arom}$); 622 (s, δ_{ClO_4}). ^{1}H-NMR (200 Mz, CD_3NO_2, ppm with reference to TMS): 3.76 (s, 24H), 5.30 (d, 4H, ^2J = 16.8 Hz), 5.70 (d, 4H, ^2J = 16.8 Hz), 6.34 (d, 8H, ^4J = 2 Hz), 6.52 (t, 4H, ^4J = 2 Hz), 7.08 (d, 4H, ^3J = 8.5 Hz), 7.36 (t, 4H, ^3J = 8.5 Hz), 7.38 (d, 4H, ^3J = 8.5 Hz), 7.50 (t, 4H, ^3J = 8.5 Hz), 7.98 (d, 4H, ^3J = 8.5 Hz), 8.28 (t, 4H, ^3J = 8.5 Hz). UV−vis (propylene carbonate, cm^{-1}): 30 826 (ϵ = 48 820 M^{-1} cm^{-1}), 32 701 (50 660), 35 112 (44 060). FAB-MS (9 kV): m/z 1537 $[Ag_2(L^4)_2(ClO_4)]^+$, 720 $[Ag_2(L^4)_2]^{2+}$.

A solution of 39.5 mg of L^8 (0.05 mmol) in 3 mL of CH_2Cl_2/MeCN, 2:1 v/v, was added dropwise under stirring to 10.5 mg of $AgClO_4 \cdot H_2O$ (0.05 mmol) in 1 mL of MeCN. The resulting orange solution was stirred in the dark for 1 h at room temperature, the solvents were removed, and the yellow solid residue was dried for 3 h (10^{-2} Torr, 40 °C). The solid was dissolved in MeCN, and *tert*-butyl methyl ether was diffused into the solution, yielding 78 mg of yellow crystals (yield 80%). Anal. Calcd for $C_{94}H_{94}N_{12}O_{17}Cl_2Ag_2$ (fw 1950.49): C, 57.88; H, 4.86; N, 8.62. Found: C, 57.86; H, 4.84; N, 8.64. IR (KBr, cm^{-1}): 3100, 3080 (w, $\nu_{CH\ arom}$); 2972, 2938, 2840 (w, $\nu_{CH\ aliph}$); 1597 (vs), 1558 (m), 1532 (s, $\nu_{C=C}$, $\nu_{C=N}$); 1093 (vs, ν_{ClO_4}); 748 (m, $\delta_{CH\ arom}$); 624 (s, δ_{ClO_4}). ^{1}H-NMR (200 Mz, DMF-d_7, ppm with reference to TMS): 1.25 (t, 12H, ^3J = 7 Hz), 3.54 (q, 8H, ^3J = 7 Hz), 3.85 (s, 24H), 5.62 (s, broad, 4H), 5.88 (s, broad, 4H), 6.44 (d, 8H, ^4J = 1.5 Hz), 6.69 (d, 4H, ^4J = 1.5 Hz), 6.72 (t, 4H, ^4J = 1.5 Hz), 7.12 (d, 4H, ^3J = 8 Hz), 7.38 (m, 4H), 7.51 (m, 4H), 7.70 (d, 4H, ^3J = 8 Hz), 7.85 (s, 4H). ES-MS (MeCN): m/z 867.3 $([Ag_2(L^8)_2]^{2+})$.

Potentiometric Titrations. Stability constants of the 1:3 complexes were determined at 298.2 ± 0.1 K by a competitive potentiometric method with Ag^+.[37] To avoid any interference from water, all measurements were made under controlled atmosphere (N_2, <10 ppm of water, M. Braun glovebox, model Labmaster 130). MeCN was chosen as solvent rather than propylene carbonate or methanol/water, 95:5 v/v, because the stability constants of the silver complexes are closer to those of the lanthanide complexes in this solvent, allowing a more precise determination. The water content of the solutions was checked before and after the measurements by Karl Fischer titrations and never exceeded 50 ppm. Titrations were carried out with a Metrohm Titrino DMS 716 potentiometer (resolution 0.1 mV, accuracy 0.2 mV) linked to an IBM PS/2 computer and the following setup: $Ag/AgClO_4$ (C_{ag}), Ln^{III} (C_{Ln}), 0.1 M NEt_4ClO_4//0.1 M NEt_4ClO_4/0.09 M NEt_4ClO_4, 0.01 M $AgClO_4$/Ag. A 20 mL titration vessel (Metrohm 6.1418.220) and automatic or manual burettes (Metrohm 6.3012.223, 20 mL, accuracy 0.03 mL, or 6.3012.153, 5 mL, accuracy 0.015 mL, or EA928−5, 5 mL, accuracy 0.003 mL) were used along with Metrohm electrodes 6.0718.000 (reference) and 6.0331.050 (measurement). Calibration of the silver electrode, performed before each titration, revealed a Nernstian behavior between 5×10^{-6} and 2×10^{-3} M, both in absence (slope 63.6 ± 0.2) and in presence of Ln^{III} cations (slope 58.5 ± 0.7). Three different experimental procedures were used in order to achieve the best reproducibility: (A) $AgClO_4$ and $Ln(CF_3SO_3)_3$ in a 1:1 ratio (*ca.* 3×10^{-4} M) were titrated by a solution of 1.7×10^{-3} M L^i; (B, C) a solution of Ln^{III} (*ca.* 6×10^{-4} M) and L^i in a 1:2 (B) or 1:3 (C) ratio was titrated by Ag^I until Ag^I:Ln^{III} reached 1:2.5. The data (150−200 points per titration curve, drift <0.5 mV/min, delay <200 s between points) were mathematically treated by the program SUPERQUAD.[41] Each titration was repeated two to five times.

Spectrophotometric Titrations. Electronic spectra in the UV−visible range were recorded at 293 K from 10^{-3} mol dm^{-3} acetonitrile solutions with Perkin-Elmer Lambda 5 and Lambda 7 spectrometers connected to an external computer and using quartz cells of 0.1 cm path length. In a typical experiment, 50 mL of L^1 in acetonitrile (*ca.* 10^{-4} M) was titrated with 10^{-3} M Ln^{III} in acetonitrile. After each addition of 0.20 mL, the absorbances at 10 different wavelengths were measured and transferred to the computer. Factor analysis and stability constant determination were carried out as previously described[42] or by using the program SPECFIT;[43] both procedures gave identical results. For the titration of L^7 by Eu^{III} (298 K), smaller volumes were added around the Eu^{III}:L^7 ratios 1:3, 1:2, and 1:1 and absorbances at 320 wavelengths were taken into account.

Other Physicochemical Measurements. IR spectra were obtained from KBr pellets with a Perkin-Elmer 883 or a Mattson Alpha Centauri FT spectrometer. ^{1}H-NMR spectra were recorded at 25 °C on Varian Gemini 300 and Varian XL200 broad-band spectrometers. Spin−lattice relaxation times (T_1) were obtained with the inversion-recovery technique on degassed solutions using 16−20 variable delay times t_D. Nonlinear least-squares fits of the monoexponential magnetization decays gave T_1 values which were the average of two or three independent measurements. Electron ionization mass spectra (70 eV) were obtained with VG 7000E and Finnigan 4000 instruments. Pneumatically-assisted electrospray (ES-MS) mass spectra were recorded from 10^{-4} M solutions in acetonitrile on an API III tandem mass spectrometer (PE Sciex) by infusion at 4−10 μL min^{-1}.[29] Cyclic voltammograms were recorded using a BAS CV-50W potentiostat and a three-electrode system consisting of a stationary Ag disk working electrode (Metrohm 6.0331.050), a Pt counter electrode, and a non-aqueous reference electrode similar to the one used for potentiometric titrations. NEt_4ClO_4 (0.1 M in CH_3CN) served as an inert electrolyte.

(40) Bochet, C. G.; Piguet, C.; Williams, A. F. *Helv. Chim. Acta* **1993**, *76*, 372.
(41) Sabatini, A.; Vacca, A.; Gans, P. *Coord. Chem. Rev.* **1992**, *120*, 389.
(42) Piguet, C.; Bernardinelli, G.; Bocquet, B.; Quattropani, A.; Williams, A. F. *J. Am. Chem. Soc.* **1992**, *114*, 7440.
(43) Gampp, H.; Maeder, M.; Meyer, C. J.; Zuberbühler, A. D. *Talanta* **1986**, *33*, 943.

Table 1. Crystallographic Data for $[Yb(OH)(L^1)_2]_2(ClO_4)_4(HClO_4)_{0.5}(CH_3CN)_{7.32}(L^1)_{0.5}$ (**1**)

formula	$C_{109.14}H_{100.96}N_{29.82}O_{20}Cl_{4.5}Yb_2$
fw	2655.92
cryst system	triclinic
space group	$P\bar{1}$
a (Å)	13.250(2)
b (Å)	16.329(2)
c (Å)	27.653(3)
α (deg)	99.941(9)
β (deg)	93.394(9)
γ (deg)	108.114(9)
V (Å^3)	5560.5(10)
Z	2
T (°C)	−93(2)
λ (Å)	0.710 73
D_{calc} (g cm^{-3})	1.586
$\mu_{Cu\ K\alpha}$ (cm^{-1})	18.63
$F(000)$	2682
θ range (deg)	1.63−24.08
index range h	$-15 \le h \le 15$
index range k	$-18 \le k \le 18$
index range l	$-31 \le l \le 31$
no. of reflns collectd	35 004
no. of indpnt reflns, $I > 2\sigma_I$	16 390
goodness of fit on F^2	1.065
R^a	0.0478
$R_w{}^b$	0.1344

[a] $R = \sum[|F_o| - |F_c|]/\sum|F_o|$. [b] $R_w(F_o^2) = [\sum w(F_o^2 - F_c^2)^2/\sum w(F_o^4)]^{1/2}$.

The reference potential ($E° = +0.35$ V *vs* SCE) was standardized against 10^{-3} M $[Ru(bipy)_3](ClO_4)_2$. The scan speed used was 100 mV s^{-1}, and voltammograms were analyzed according to established procedures.[44] Elemental analyses were performed by Dr. H. Eder of the Microchemical Laboratory of the University of Geneva.

X-ray Experimental Details. The yellow crystal to be measured was dipped in a drop of Hostinert 216 and frozen at 180 K. The data collection took place on a Stoe IPDS system equipped with Mo radiation. Two hundred images were exposed during 5 min each. An inspection of reciprocal space ascertained that the diffraction figure consisted essentially of the spots corresponding to the cell given in Table 1. The intensities were corrected for Lorentz and polarization effects. The decay during the measurement was negligible. The structure was solved with the help of SHELXTL 5.05,[45] and some corollary calculations were performed by means of XTAL[46] and PACHA.[47] All non-hydrogen atoms of the dinuclear complex, the coordinated ligands, and some of the solvent molecules were refined anisotropically, but the atoms of the disordered free ligand and acetonitrile molecules were kept isotropic. For one of them, a population parameter could be refined (N73). Most of the residuals, of which none was larger than 2.9 e Å^{-3}, lay near the Yb cations, the disordered solvent molecules, or the hydrogen-bearing atoms. Only two of the last ones were included in the refinement: the two peaks of ~0.5 e Å^{-3} near the bridging oxygen atoms. They converged to very reasonable positions, but the IDP for H1 had to be kept constant in order to prevent it from becoming negative; in fact the IDP values of both H1 and H2 were set to 0.02 Å^2. Despite this slight problem, it appears clearly that the Yb^{III} ions are bridged by hydroxo groups. One of the oxygen atoms of a perchlorate, O33, was clearly farther away form its chlorine than any of the other ones; its distance of 1.55 Å led us to interpret this Cl,O group as a perchloric acid molecule rather than a perchlorate. Some restraints were imposed on the disordered ligand and solvent molecules so as to enforce their geometries (the N≡C and N−C distances were set to the average values of the better defined acetonitrile molecules, and flatness criteria were applied to the benzimidazole and pyridine rings of the disordered ligand).

Results

Thermodynamic Properties of the Complexes with L^1. Spectrophotometric titrations of ligand L^1 by lanthanide perchlorates[27] show that successive complexes $[Ln(L^1)_i]^{3+}$ (i = 1−3) form in acetonitrile for all lanthanides and that 1:3 complexes with the heavier lanthanides (Ho−Lu) display a significant lower stability than those with lighter Ln^{III} ions. The stability constants extracted from both spectrophotometric and potentiometric titrations are reported in Table 2. For spectrophotometric titrations, factor analysis pointed to the presence of four absorbing species and all data were fitted by a least-squares procedure to the following equilibria:

$$Ln^{3+} + L^i \rightleftharpoons [Ln(L^i)]^{3+} \qquad \log K_1$$

$$[Ln(L^i)]^{3+} + L^i \rightleftharpoons [Ln(L^i)_2]^{3+} \qquad \log K_2 \qquad (1)$$

$$[Ln(L^i)_2]^{3+} + L^i \rightleftharpoons [Ln(L^i)_3]^{3+} \qquad \log K_3$$

$\log K_1$ is more or less constant over the Ln^{III} series (average 9.0 ± 0.3) and so is $\log K_2$, with the exception of the values for lanthanum and lutetium, which are respectively slightly larger and smaller than the average calculated without these data (7.0 ± 0.3). The difference between $\log K_1$ and $\log K_2$ ($\log(K_1/K_2) \approx 2$) is approximately twice that expected from the statistical evaluation ($\log(K_1/K_2) = 0.78$),[48] taking into account a tricapped trigonal prismatic (ttp) polyhedron and imposing the condition that the capping positions always be occupied by the N atom from the central pyridine, as observed in the crystal structures of several 1:1,[24,25] 1:2,[27,49] and 1:3 complexes.[26,27] The formation of the triple-helical complexes $[Ln(L^1)_3]^{3+}$ follows another trend, $\log K_3$ staying relatively constant up to terbium and then decreasing substantially with decreasing ionic radii of the Ln^{III} ions. Comparing $\log(K_2/K_3)$ with its statistical value (0.48),[48] it appears that the 1:3 complexes are favored for the intermediate Ln^{III} ions. However, strong correlation between the UV spectra of the three successive complexes induces large uncertainties in the calculation of the successive stability constants, which prevents a more detailed interpretation. We have therefore reinvestigated these systems using competitive potentiometric titrations with Ag^I in order to determine $\log K_3$ more precisely.[37]

The reaction of Ag^I with L^1 in acetonitrile leads to the exclusive formation of a double-stranded helicate $[Ag_2(L^1)_2]^{2+}$ as ascertained by UV−visible, ^{1}H-NMR, and ES-MS spectra.[50,51] In particular, the ^{1}H-NMR spectrum reflects the presence of a D_2-symmetrical helicate in solution, very similar to $[Cu_2(L^1)_2]^{2+}$,[50,51] except that the protons from the methyl groups appear to be less shielded than in the copper dimer, a possible consequence of the reduced interstrand stacking interaction induced by the larger Ag^I ion. The direct potentiometric titration of L^1 by $AgClO_4$ in dried acetonitrile (0.1 M Et_4NClO_4, 25 °C, 26 ppm of H_2O) confirms the formation of the dimer $[Ag_2$-

(44) Bard, A. J.; Faulkner, L. R. *Electrochemical Methods, Fundamentals and Applications*; John Wiley: New York, Chichester, Brisbane, Toronto, Singapore, 1980.
(45) *SHELXTL 5.05*; Siemens Analytical X-Ray Instruments Inc.: Madison, WI, 1996.
(46) Hall, S. R.; Stewart, J. M. *XTAL 3.2 User's Manual*; Universities of Western Australia and Maryland: Nedlands, Australia, and College Park, MD, 1992.
(47) Henry, M. *PACHA: Partial Atomic Charge Analysis*; Université Louis Pasteur: F-67000 Strasbourg, France, 1993.
(48) Beck, M. T.; Nagypal, I. *Chemistry of Complex Equilibria*; Ellis Horwood: Chichester, U.K., 1990.
(49) Wang, S.; Zhu, Y.; Gao, Y.; Wang, L.; Luo, Q. *J. Chem. Soc., Dalton Trans.* **1994**, 2523.
(50) Williams, A. F.; Piguet, C.; Carina, R. In *Transition Metals in Supramolecular Chemistry*; Fabbrizzi, L., Poggi, A., Eds.; Kluwer Academic: Dordrecht, Boston, London, 1994; pp 409−24.
(51) Rüttimann, S.; Piguet, C.; Bernardinelli, G.; Bocquet, B.; Williams, A. F. *J. Am. Chem. Soc.* **1992**, *114*, 4230.

Table 2. Stability Constants of $[Ln(L^i)_n]^{3+}$ Complexes

	ligand L^1					ligand L^4		ligand L^8
Ln	log K_1[a]	log K_2[a]	log K_3[a]	log β_3[a]	log K_3[b,c]	log K_2[b,g]	log K_3[b,g]	log K_3[b,d]
La	8.9 ± 0.3	7.9 ± 0.4	6.5 ± 0.6	23.3 ± 0.9	5.8 ± 0.2	5.0 ± 0.1	2.2 ± 0.2	4.8 ± 0.2
Ce					6.0 ± 0.1	4.8 ± 0.1	2.9 ± 0.3	
Pr					6.3 ± 0.1	4.9 ± 0.1	2.8 ± 0.1	5.5 ± 0.2
Nd	8.7 ± 0.2	7.2 ± 0.4	7.3 ± 0.6	23.2 ± 0.8	6.5 ± 0.2	4.9 ± 0.1	3.2 ± 0.2	
Sm					6.4 ± 0.2	5.5 ± 0.1	3.6 ± 0.1	6.0 ± 0.1
Eu	9.0 ± 0.2	6.7 ± 0.3	6.9 ± 0.4	22.6 ± 0.6	*e*	*e*	*e*	*e*
Gd	8.5 ± 0.2	6.7 ± 0.4	6.9 ± 0.5	22.1 ± 0.8	6.6 ± 0.2	4.8 ± 0.1	3.2 ± 0.1	6.1 ± 0.2
Tb	9.3 ± 0.3	7.1 ± 0.5	7.6 ± 0.8	22 ± 1	6.1 ± 0.1	4.9 ± 0.1	3.1 ± 0.1	5.9 ± 0.1
Dy					5.8 ± 0.1			5.2 ± 0.2
Ho	8.9 ± 0.3	7.3 ± 0.5	6.1 ± 0.6	22 ± 1	5.3 ± 0.1			4.8 ± 0.2
Er					4.7 ± 0.2	5.1 ± 0.1	3.0 ± 0.1	
Tm					3.9 ± 0.1			3.9 ± 0.1[f]
Yb	9.4 ± 0.5	7.1 ± 0.6	5.2 ± 0.7	22 ± 1	3.4 ± 0.1			3.1 ± 0.1[f]
Lu	9.0 ± 0.4	6.4 ± 0.4	4.9 ± 0.5	20.3 ± 0.9	2.7 ± 0.1	5.4 ± 0.1	2.9 ± 0.1	

[a] Spectrophotometric titration at 20 ± 0.1 °C in acetonitrile (root-mean-square difference between observed and calculated absorbances <0.006). [b] Competitive potentiometric titration at 25 ± 0.1 °C in anhydrous acetonitrile, in presence of 0.1 M Et_4NClO_4. [c] log K_1 (≥9) and log K_2 (≥7) were fixed (see text). [d] log K_1 (≥9) and log K_2 (≥7) were fixed, except for those of Tm and Yb (see text). [e] Not measurable since Ag(s) reduces Eu^{III}. [f] log K_2 = 7.0 ± 0.1 (Tm) and 6.8 ± 0.2 (Yb). [g] log K_1 was fixed (≥9, see text).

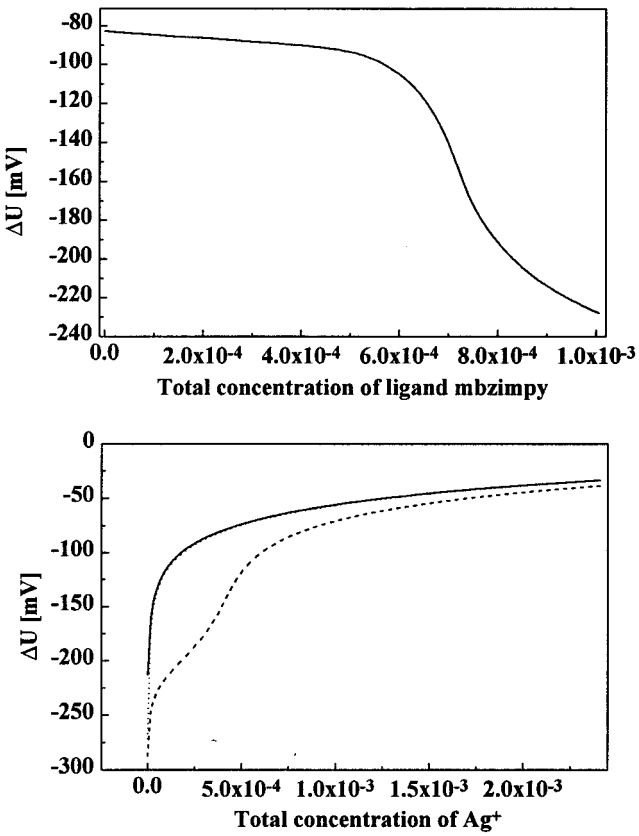

Figure 1. Top: Potentiometric titration of Ag^I/Ce^{III} by L^1 at 25 °C, I = 0.1 M (Et_4NClO_4). Initial concentrations: $[Ag^I] = [Ce^{III}] = 3.34 \times 10^{-4}$ M; $[L^1] = 1.758 \times 10^{-3}$ M. Bottom: Potentiometric titrations of Lu^{III}/L^1 by Ag^I at 25 °C, I = 0.1 M (Et_4NClO_4). Initial concentrations: $[L^1] = 1.235 \times 10^{-3}$ M; $[Lu^{III}] = 6.17 \times 10^{-4}$ M (dotted line) and 4.52×10^{-4} M (dashed line); $[Ag^I] = 9.593 \times 10^{-3}$ M. The solid line represents the calibration curve of the Ag^I electrode in the presence of Lu^{III}.

$(L^1)_2]^{2+}$ as the only significant complex in solution with log β_{22} = 13.9 ± 0.1, while the mean value extracted from the

$$2L^i + 2Ag^+ \rightleftharpoons [Ag_2(L^i)_2]^{2+} \qquad \log \beta_{22} \qquad (2)$$

titrations of Ln^{III}-containing solutions is 14.2 ± 0.2. The potentiometric competitive titrations of mixtures of Ag^I and Ln^{III} by L^1 (Figure 1) show little variation of the electrical potential with respect to the Ag calibration curve for low L^1:Ln^{III} ratios, in line with the preferential formation of $[Ln(L^1)_i]^{3+}$ (i = 1, 2); when a L^1:Ln^{III} ratio of 3 is approached, the potential decreases substantially (typically 120 mV), reflecting the competition between $[Ln(L^1)_3]^{3+}$ and $[Ag_2(L^1)_2]^{2+}$. Titration of $[Ln(L^1)_n]^{3+}$ complexes by Ag^I confirmed the large stability of the complexes with n = 1 or 2, the potential curve being almost identical with the Ag^I calibration curve (Figure 1). All potentiometric data were fitted to the four equations (1) and (2) because (i) this model gave the smallest residuals and (ii) an ES-MS study of the mixed $Gd^{III}/Ag^I/L^1$ system demonstrated clearly the absence of any mixed Gd−Ag complexes and the presence of the predominant species $[Ag_2(L^1)_2]^{2+}$ for Ag^I and $[Gd(L^1)_n]^{3+}$ (n = 2, 3) for Gd^{III} (traces of $[Ag(L^1)_2]^+$ are only observed in presence of a large excess of L^1). However, it turned out that for most investigated systems, the fit on K_3 was insensitive to the values of K_1 and K_2 within several orders of magnitude, so that these were fixed to respectively log $K_1 \geq 9$ and log $K_2 \geq 7$ in the last iterations. The water content of the solutions (determined before and after the titrations) was between 30 and 50 ppm, corresponding to approximately 1−2 molecules of water per Ln^{III} ion. Since water has a high affinity for Ln^{III} ions, we have checked the influence of added water (30−170 ppm) on log K_3 for Sm^{III}. log β_{22}(Ag) appeared to be insensitive to the amount of added water but log K_3(Sm^{III}) decreased by approximately 0.1 unit per 11 ppm of added water until 120 ppm and decreased more sharply between 120 and 170 ppm. In the range 30−50 ppm, the decrease was only 0.2 unit, comparable to the experimental error on log K_3 (Table 2), so that no correction was applied to the reported figures. The general trend for log K_3 follows the one evidenced from the spectrophotometric data with, however, discrepancies toward the end of the lanthanide series: the potentiometric data are smaller by 1−2 units, but they are much more precisely defined (±0.1−0.2 unit) compared to the values extracted from the optical spectra (±0.5−0.8 unit); part of these discrepancies may arise from the fact that spectrophotometric titrations have been carried out at variable ionic strength. In the beginning of the series, log K_3 increases from 5.8 (La) to 6.5 (Nd), reflecting the increase in electron density of the cations, then levels off, and decreases sharply from Gd (6.6) to Lu (2.7). The large size-discriminating effect of L^1, Δ log(Gd−Lu) ≈ 4, is noteworthy (Figure 2). The previously reported X-ray crystal structure of $[Eu(L^1)_3]^{3+}$ shows that the Eu^{III} ion is imbedded into a tight cavity,[27] which is difficult to shrink to accommodate

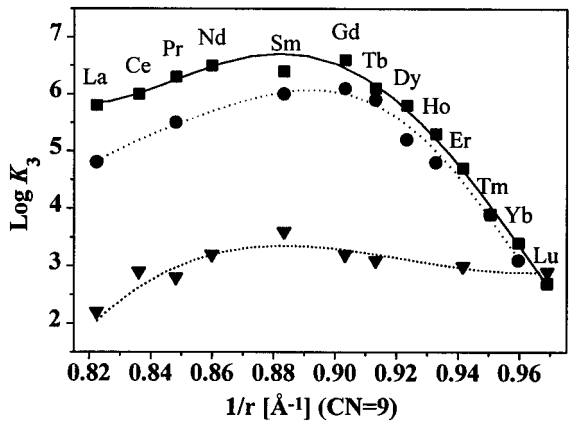

Figure 2. Third stability constant for the formation of lanthanide triple helicates with ligands L^1 (squares), L^4 (triangles), and L^8 (circles) as determined by competitive potentiometric titration at 25 ± 0.1 °C, I = 0.1 M, versus the reciprocal of the ionic radii for a coordination number of 9.[5]

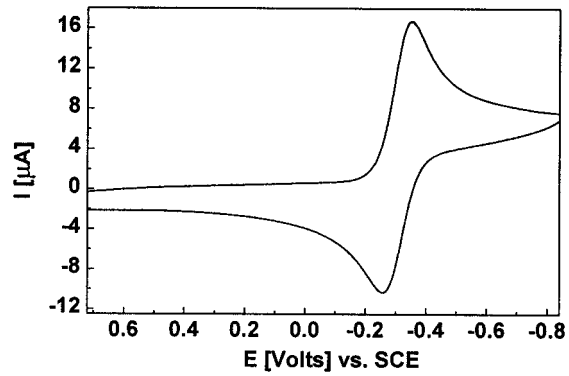

Figure 3. Cyclic voltammogram of a solution of $[Eu(L^1)_3](ClO_4)_3$ 10^{-3} M in dry MeCN (I = 0.1 M, scan rate = 100 mV/s).

smaller lanthanide ions without inducing large steric constraints, a fact exemplified in the log K_3 versus $1/r_i$ dependence if we are able to demonstrate that the solid state structure is retained in solution (*vide infra*). Stability with podands usually increases monotonically with Z, e.g. edta with Δ log(Lu−La) ≈ 4.3,[5] while size-discriminating effects have been essentially reported for macrobicyclic ligands, viz. cryptand (2,2,2) in propylene carbonate with Δ log(Sm−La) ≈ 3.1.[52]

Potentiometric data for Eu^{III} could not be obtained because of its reduction to Eu^{II}. We have studied the latter process by cyclic voltammetry in MeCN, in the presence of 0.1 M Et_4NClO_4, with a Pt disk working electrode and an Ag reference electrode (Figure 3). The peak separation is 96 mV and reflects the quasireversibility of the Eu^{III}/Eu^{II} system. The formal reduction potentials versus SCE in the presence (3 equiv) and in the absence of L^1 amount to −320 ($E^{\circ\prime}_L$) and +140 mV ($E^{\circ\prime}_S$). These measured reduction potentials are directly related to the stability constants $\beta_3^{Eu(III)}$ and $\beta_3^{Eu(II)}$ through the relationship $E^{\circ\prime}_L - E^{\circ\prime}_S = 0.059 \log(\beta_3^{Eu(II)}/\beta_3^{Eu(III)})$, yielding $\log(\beta_3^{Eu(III)}/\beta_3^{Eu(II)}) = 7.8$, that is $\log \beta_3^{Eu(II)} \approx 15$. The approximate 460 mV anodic shift of the Eu^{III}/Eu^{II} process upon formation of the complex $[Eu(L^1)_3]^{3+}$ mainly originates in an electrostatic effect associated with the replacement of nitrile donors in $[Eu(NCCH_3)_n]^{3+}$ with electron-donor imine groups in $[Eu(L^1)_3]^{3+}$.[53] This value can be compared with the 830 mV

Table 3. Chemical Shifts of the Triple-Helical Complexes $[Ln(L^1)_3]^{3+}$ in Solution 5 × 10^{-3} M in CD_3CN (ppm with Respect to TMS, 298 K)[a]

Ln	H^1	H^2	H^3	H^4	H^5	H^6	$R^2 = CH_3$
Y	6.84	6.79	7.33	7.68	7.68	7.80	3.89
La	7.15	6.80	7.34	7.71	7.71	7.91	3.77
Ce	2.42	6.35	7.46	8.48	9.51	9.51	5.15
Pr	−2.80	5.80	7.55	9.40	11.98	11.16	6.76
Nd	0.83	6.16	7.45	9.11	10.16	10.28	5.75
Sm	5.77	6.69	7.37	7.81	8.02	8.11	4.18
Eu	13.27	7.52	7.31	5.71	2.88	4.92	1.86
Tb	−51.90	0.67	9.16	11.74	18.36	17.01	20.01
Dy	−70.51	−1.63	9.23	14.31	22.64	22.65	25.43

Ln	C^1	C^2	C^3	C^4	C^5	C^6	$R^2 = CH_3$
Y	119.51	126.44	127.04	112.64	126.60	142.57	34.48
La	119.82	126.49	127.19	112.34	127.01	142.75	34.43
Ce	118.15	125.87	127.05	113.41	133.45	143.85	36.34
Pr	116.62	124.93	127.25	114.75	144.50	144.85	38.59
Nd	118.88	125.02	127.34	114.76	147.69	141.45	37.58
Sm	119.12	126.51	127.08	112.55	126.79	143.25	34.83
Eu	117.80	129.47	125.89	109.08	89.34	150.80	30.21
Tb	88.21	126.10	125.27	112.65	62.32	201.48	46.54
Dy	90.10	121.79	124.63	115.97	72.43	196.18	53.14

[a] See Chart 1 for the numbering scheme.

shift found for $[EuFe(L^{10})_3]^{5+}$, where Eu^{III} occupies an analogous nine-coordinate ttp site except for the replacement of the terminal benzimidazole side arms by carboxamide groups.[28] It thus appears that aromatic N-heterocyclic donors are suitable for Eu^{II} and the three helically wrapped L^1 ligands provide a cavity which easily accommodates Eu^{II} whose ionic radius is 0.18 Å larger than Eu^{III}. This is consistent with the observation that log K_3 decreases only marginally in going from the midrange lanthanide ions to the lighter Ln^{III} cations.

Structural Properties of the Complexes with L^1. In order to unravel the origin of the thermodynamic size-discriminating effect observed in solution, we have resorted to NMR to gain information on the solution structure of the $[Ln(L^1)_3]^{3+}$ complexes. We have previously shown that the 1:3 complexes $[Ln(L^i)_3]^{3+}$ (i = 1, 4, 5; La = La, Eu) adopt the D_3 symmetry expected for idealized mononuclear triple-helical complexes, but no accurate structural parameter has been determined.[26,27] The paramagnetic NMR of axial Ln^{III} complexes is ideally suited for the investigation of solution structures since both structural (*via* the pseudocontact term) and electronic (*via* the contact term) parameters can be readily extracted from an isostructural series.[54] For the D_3−symmetrical complexes $[Ln(L^1)_3]^{3+}$ (Ln = La−Eu; 5 mM in CD_3CN), a dependable assignment of the ^1H- and ^{13}C-NMR signals was obtained from nuclear Overhauser effects (NOE) and two-dimensional homo- and heteronuclear correlation spectroscopies (Table 3). For Ln = Tb, Dy, and Y, other signals, assigned to the free ligand and $[Ln(L^1)_2]^{3+}$, appeared in the spectra (Figure 4) and became significant for Ln = Dy and Y, in agreement with the decrease of log K_3 for small Ln^{III} ions. Integration of the ^1H-NMR signals showed that $[Ln(L^1)_3]^{3+}$ corresponded to 94, 58, and 46% of the ligand speciation for respectively Ln = Tb, Dy, and Y. Although exchange processes are slow on the NMR time scale and do not significantly affect the chemical shifts in $[Ln(L^1)_3]^{3+}$, we have limited our studies to large Ln^{III} ions (Ln = La−Dy) for which the 1:3 complexes are the major products in solution.

(52) Gillain, G.; Barthelemy, P. P.; Massaux, J.; Desreux, J. F. *J. Chem. Soc., Dalton Trans.* **1984**, 2847.
(53) Smith, P. H.; Reyes, Z. E.; Lee, C.-W.; Raymond, K. N. *Inorg. Chem.* **1988**, *27*, 4154.
(54) Bertini, I.; Luchinat, C. *NMR of Paramagnetic Molecules in Biological Systems*; Benjamin/Cummings: Menlo Park, CA, 1986. Sherry, A. D.; Geraldes, C. F. G. C. In *Lanthanide Probes in Life, Chemical and Earth Sciences*; Bünzli, J.-C. G., Choppin, G. R., Eds.; Elsevier: Amsterdam, 1989; Chapter 4.

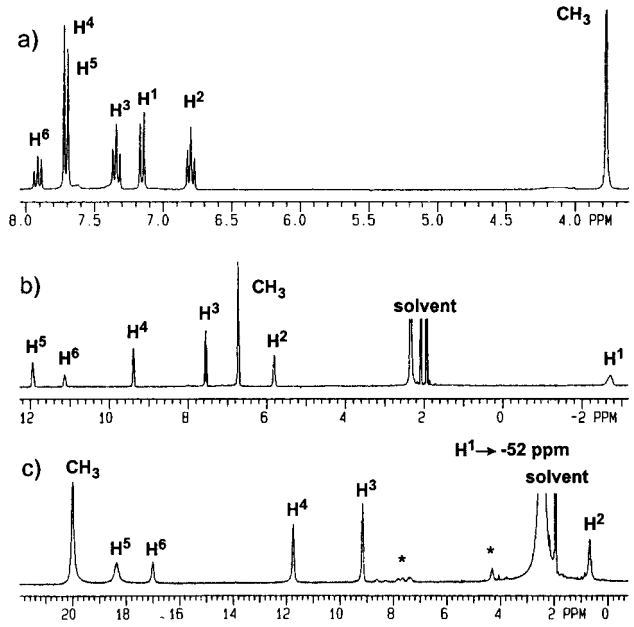

Figure 4. Parts of the ^{1}H-NMR spectra of $[Ln(L^1)_3]^{3+}$ in CD_3CN at 298 K: (a) Ln = La; (b) Ln = Pr; (c) Ln = Tb (asterisks indicate the signals of the free ligand).

As a result of the longer electronic relaxation time for Tb^{III} and Dy^{III}, no reliable NOESY and COSY spectra could be recorded.[55] The assignment of the NMR signals for these metal ions were thus based on T_1 measurements and iterative fitting processes (*vide infra*).

Further structural and electronic information may be gained from the separation of contact and pseudocontact contributions to the isotropic NMR paramagnetic shifts. The shift δ_{ij}, induced at a nucleus i of a ligand bound to a lanthanide j can be expressed as the sum of the diamagnetic shift δ_i^{dia} (estimated from the shift of $[La(L^1)_3]^{3+}$ for Ln = Ce−Nd and $[Y(L^1)_3]^{3+}$ for Ln = Sm−Dy), the contact shift δ_{ij}^{c} (associated with through-bond Fermi interactions),[56] the pseudocontact shift δ_{ij}^{pc} (associated with the anisotropic part of the axial magnetic susceptibility tensor),[57] and the shift due to the bulk magnetic susceptibility δ_j^{bulk} (eq 3).[58] δ_j^{bulk} can be estimated from eq 4, which applies

$$\delta_{ij} = \delta_i^{dia} + \delta_{ij}^{c} + \delta_{ij}^{pc} + \delta_j^{bulk} \quad (3)$$

$$\delta_j^{bulk} = \frac{4\pi C}{3T}\left(\frac{\mu_{eff}}{2.84}\right)^2 \quad (4)$$

to a superconducting solenoid,[59] where C is the concentration (mM) of Ln^{III}, μ_{eff} is the effective magnetic moment for Ln^{III} (taken for the free ion in μ_B) and T is the temperature (K). However, as the chemical shifts are measured with respect to internal TMS, the contribution of δ_j^{bulk} is zero. The isotropic paramagnetic contribution δ_{ij}^{iso} is thus given by eq 5, which

$$\delta_{ij}^{iso} = \delta_{ij} - \delta_i^{dia} = \delta_{ij}^{c} + \delta_{ij}^{pc} = F_i\langle S_z\rangle_j + G_i C_j \quad (5)$$

allows a straightforward separation of contact and pseudocontact terms F_i and G_i[29,60] for a given nucleus i in an isostructural series of Ln^{III} complexes since values of the lanthanide-dependent terms $\langle S_z\rangle_j$ and C_j have been tabulated.[56,57] A multilinear least-squares fit of the experimental isotropic paramagnetic shifts (δ_{ij}^{iso}) for $[Ln(L^1)_3]^{3+}$ (Ln = Ce−Eu) to eq 3 provides a first set of F_i and G_i values which are then used in eqs 3 and 5 to predict the NMR shifts (δ_{ij}) of $[Ln(L^1)_3]^{3+}$ (Ln = Tb, Dy). The calculated spectra were in good agreement with the experimental shifts, leading to a dependable assignment of the ^{1}H- and ^{13}C-NMR signals for these strongly paramagnetic cations. A second fitting process with the complete data (Ln = Ce−Dy) leads to the final F_i and G_i terms and agreement factors AF_i[29,60] given in Table 4 (the corrected contact and pseudocontact contributions are given in the Supporting Information, Table S1). The agreement factors for ^{1}H and ^{13}C nuclei are satisfying ($004 < AF_i < 0.25$) and can be compared with similar mathematical treatments applied to analogous 1:3 complexes $[Ln(pyridine\text{-}2,6\text{-}dicarboxylato)_3]^{3-}$ ($0.004 < AF_i < 0.27$)[60] and $[Ln(pyridine\text{-}2,6\text{-}bis(N,N\text{-}diethylcarboxamido)_3)]^{3+}$ ($0.01 < AF_i < 0.31$).[61] This result suggests that the complexes $[Ln(L^1)_3]^{3+}$ (Ln = Ce−Dy) are isostructural in solution, which is confirmed by the straight lines observed for plots of $\delta_{ij}^{iso}/\langle S_z\rangle_j$ vs $C_j/\langle S_z\rangle_j$ (eq 6) and δ_{ij}^{iso}/C_j vs $\langle S_z\rangle_j/C_j$ (eq 7) for each ^{1}H and ^{13}C nucleus (eqs 6 and 7 correspond to linear forms of eq 5).[54,58]

$$\frac{\delta_{ij}^{iso}}{\langle S_z\rangle_j} = F_i + G_i\frac{C_j}{\langle S_z\rangle_j} \quad (6)$$

$$\frac{\delta_{ij}^{iso}}{C_j} = F_i\frac{\langle S_z\rangle_j}{C_j} + G_i \quad (7)$$

The sizable F_i values of H^1 (−0.41) and H^5 (0.42) demonstrate a significant spin delocalization onto the coordinated aromatic rings of L^1 which is larger than that found in $[LnZn(L^9)_3]^{3+}$ (−0.26 and 0.34), where similar but substituted tridentate units are bound to Ln^{III}.[31] The pseudocontact terms only depend on the geometric position of the nucleus i (eq 8; r_i and θ_i are the internal axial coordinates with respect to the ligand field axes) for a particular ligand field constant (a) and a given temperature.[60]

$$G_i = \frac{a}{T^2}\frac{1 - 3\cos^2\theta_i}{r_i^3} \quad (8)$$

Since G_i values depend on both r_i and θ_i, it is difficult to extract atomic positions from the fitting process. Of particular interest are the G_i values close to zero since they correspond to $\theta_i \approx 54.7°$ ($G_i(C^3)$, $G_i(H^3)$) and allow the detection of small structural variations between the solid state and solution structures.[61] For $[Ln(L^1)_3]^{3+}$ (Ln = Ce−Dy), negative values are found for $G_i(H^6)$ and $G_i(C^6)$ ($\theta_i = 90°$), which implies that $\theta_i(H^3)$ is slightly larger than 54.7° (because $G_i(H^3) < 0$) while $\theta_i(C^3)$ is smaller than 54.7° ($G_i(C^3) > 0$; Table 4). The average θ_i angles calculated from the crystal structure of $[Eu(L^1)_3]^{3+}$ are 57.8(7)° for C^3 and 59.0(9) for H^3 and are in qualitative good agreement with those obtained in solution, which suggests that the triple-helical structure is essentially retained in solution

(55) Lisowski, J.; Sessler, J. L.; Lynch, V.; Mody, T. D. *J. Am. Chem. Soc.* **1995**, *117*, 2273.
(56) Golding, R. M.; Halton, M. P. *Aust J. Chem.* **1972**, *25*, 2577.
(57) Bleaney, B. J. *J. Magn. Reson.* **1972**, *8*, 91. Reuben, J.; Rigavish, G. A. *J. Magn. Reson.* **1980**, *39*, 421.
(58) Caravan, P.; Mehrkhodavandi, P.; Orvig, C. *Inorg. Chem.* **1997**, *36*, 1316.
(59) Peters, J. A.; Huskens, J.; Raber, D. J. *Prog. NMR Spectrosc.* **1996**, *28*, 283.
(60) Reilley, C. N.; Good, B. W.; Desreux, J. F. *Anal Chem.* **1975**, *47*, 2110.
(61) Renaud, F.; Piguet, C.; Bernardinelli, G.; Bünzli, J.-C. G.; Hopfgartner, G. *Chem. Eur. J.* **1997**, *3*, 1646, 1660.

Table 4. Values for Contact (F_i) and Pseudocontact (G_i) Terms and Agreement Factors (AF_i) for ^1H and ^{13}C Nuclei in Paramagnetic Complexes $[Ln(L^1)_3]^{3+}$ (Ln = Ce−Dy) in CD_3CN at 298 K Computed by Using Eq 5[29,60]

	H^1	H^2	H^3	H^4	H^5	H^6	$R^2 = CH_3$
F_i	−0.41(12)	−0.05(2)	−0.006(5)	0.16(1)	0.42(6)	0.26(4)	0.14(3)
G_i	0.87(4)	0.094(7)	−0.008(2)	−0.111(3)	−0.30(2)	−0.22(1)	−0.25(1)
AF_i	0.04	0.06	0.05	0.06	0.10	0.08	0.05
	C^1	C^2	C^3	C^4	C^5	C^6	$R^2 = CH_3$
F_i	0.26(10)	−0.26(4)	0.07(3)	0.33(2)	3.38(19)	−0.93(14)	0.36(3)
G_i	0.25(3)	0.11(1)	0.002(9)	−0.124(7)	−0.46(6)	−0.30(5)	−0.28(1)
AF_i	0.08	0.25	0.25	0.12	0.07	0.06	0.06

except for a slight straightening of the coordinated ligands along the C_3 axis.

To substantiate this observation, we have applied a simplified form of the Solomon−Bloembergen−Morgan equation[62] for the estimation of of Ln−C^i and Ln−H^i distances in $[Ln(L^1)_3]^{3+}$. Assuming a pure paramagnetic dipolar relaxation mechanism, eq 9 holds,[62] where r_i is the Ln−nucleus i distance, r_{ref} is a

$$r_i = r_{ref}\left(\frac{T_{1c}^{\ i}}{T_{1c}^{\ ref}}\right)^{1/6} \tag{9}$$

reference distance (taken as the C_3-averaged distance of the nucleus with the largest distance from the Ln^{III} center), and T_{1c}^{i} and T_{1c}^{ref} are the longitudinal relaxation times corrected for diamagnetic relaxation according to eq 10 (T_{1dia}^{i} are the

$$\frac{1}{T_{1c}^{\ i}} = \frac{1}{T_1^{\ i}} - \frac{1}{T_{1dia}^{\ i}} \tag{10}$$

relaxation times measured for the diamagnetic complexes $[La(L^1)_3]^{3+}$; cf. Table S2, Supporting Information).

Among the light Ln^{III} cations (Ln = La−Dy), Ce^{III} possesses the largest relative dipolar contribution and the distances calculated using eqs 9 and 10 for $[Ce(L^1)_3]^{3+}$ are reported in Table 5 (Ln−C^3 and Ln−H^3 distances are taken from the X-ray crystal structure of $[Eu(L^1)_3]^{3+}$ and used as references).[27] We observe a satisfying correlation between the Ln−H^i and Ln−C^i distances found in the solid state and in solution, which confirms a similar triple-helical structure in both states.

Finally, we have used the method developed by Kemple and co-workers[63] to compare the solid state and solution structures. Starting from the C_3-average internal axial coordinates θ_i and r_i for each nucleus (taken from the X-ray crystal structure of $[Eu(L^1)_3]^{3+}$),[27] the experimental paramagnetic isotropic shifts (δ_{ij}^{iso}) of complexes $[Ln(L^1)_3]^{3+}$ are fitted to eq 11 with 11

$$\delta_{ij}^{\ iso} = \xi\chi_j^{zz}\left(\frac{1 - 3\cos^2\theta_i}{r_i^{\ 3}}\right) + \sum_i \delta_{ij}^{\ c} \tag{11}$$

parameters for each lanthanide j (13 × 11 fits; $\xi\chi_j^{zz}$, δ^c-($C^{1,2,4,5,6,R2}$), δ^c($H^{1,4,5,6}$); contact contributions are neglected for H^2, H^3, and C^3, which are sufficiently remote from Ln^{III}).[29,63] The multilinear least-squares fit allows the simultaneous calculation of (i) the experimental axial anisotropic susceptibility parameter $\xi\chi_j^{zz}$ for the complex $[Ln(L^1)_3]^{3+}$ and (ii) the contact contributions δ_{ij}^{c} given in Table S3 (Supporting Information).[63]

The average F_i and G_i terms calculated from the contact and pseudocontact contributions obtained by this method (Table S3), and using eq 5 and theoretical values of $\langle S_z\rangle_j$[56] and C_j,[57] are collected in Table 6 and can be compared with those of Table 4, for which no prerequisite structural model is involved. The qualitative good agreement between these two sets of data firmly establishes that (i) the crystal structure of $[Eu(L^1)_3]^{3+}$ is a suitable model for $[Ln(L^1)_3]^{3+}$ (Ln = La−Dy) in acetonitrile and (ii) strong interstrand stacking interactions between the three wrapped ligands also occur in solution.

Table 5. Estimated Ln−X^i Distances (Å) for $[Ce(L^1)_3]^{3+}$ in CD_3CN at 298 K from T_1 Measurements and Eq 9

H^i	Ce−H^i (Å)	Eu−H^i [a]	C^i	Ce−C^i (Å)	Eu−C^i [a]
H^1	3.90	4.00	C^1	*c*	4.25
H^2	6.26	6.21	C^2	6.21	5.54
H^3 (ref)	7.30	7.30	C^3 (ref)	6.26	6.26
H^4	6.63	6.80	C^4	5.40	5.95
H^5	5.42	5.62	C^5	5.15	4.81
H^6	6.23	6.43	C^6	4.66	5.34
$R^2 = CH_3$	5.96	*b*	$R^2 = CH_3$	5.05	5.76

[a] C_3-average distances calculated from the X-ray crystal structure of $[Eu(L^1)_3]^{3+}$.[27] [b] For $R^2 = CH_3$, no suitable average distance Ln−H^6 is available from the crystal structure. [c] The ^{13}C-NMR signal of C^1 is masked by the solvent.

Table 6. Values for Contact (F_i) and Pseudocontact (G_i) Terms for ^1H and ^{13}C Nuclei in Paramagnetic Complexes $[Ln(L^1)_3]^{3+}$ (Ln = Ce−Dy) in CD_3CN at 298 K Computed by Using Eq 11 and the Crystal Structure of $[Eu(L^1)_3]^{3+}$ as Model[29,63]

	H^1	H^2	H^3	H^4	$H^{'}$	H^6
F_i	−0.08	0	0	0.13	0.23	0.18
G_i	1.20	0.09	−0.05	−0.17	−0.49	−0.37
	C^1	C^2	C^3	C^4	C^5	C^6	$R^2 = CH_3$
F_i	0.27	−0.20	0	0.32	3.47	−0.96	0.25
G_i	0.57	0.09	−0.06	−0.17	−0.85	−0.65	−0.45

In order to investigate possible structural changes associated with the decrease of the Ln^{III} ionic radii for Ln = Ho−Lu, we have tried to crystallize the triple-helical 1:3 complex with Yb^{III}, but the isolated crystals turned out to be a dimer made of two 1:2 complexes bridged by hydroxide anions and having the composition $[Yb(OH)(L^1)_2]_2(ClO_4)_4(HClO_4)_{0.5}(CH_3CN)_{7.32}(L^1)_{0.5}$. Relevant data for its X-ray crystal structure are reported in Table 7, while Figure 5 displays the atom-numbering scheme. The structure consists of $[Yb(OH)(L^1)_2]_2^{4+}$ dimer cations (Figure 6), of partially disordered perchlorate anions, and of disordered uncomplexed solvent and ligand molecules (see Experimental Section). The two Yb^{III} ions are held at a distance of 3.66 Å by two bridging and symmetrically bonded hydroxyl groups. Each cation is additionally coordinated to the three donor atoms of two ligand strands and is therefore 8-coordinated. The ligand strands adopt a cisoid−cisoid conformation as observed previously for 1:1,[24,25] 1:2,[27,49] and 1:3[26,27] lanthanide complexes with similar ligands. The Yb^{III}−N distances show some asymmetry in the ligand coordination, both within a coordination sphere and between the two Yb^{III} ions. For each part of the dimer, one benzimidazole group is substantially more tightly bonded

(62) Nakamura, T.; Miyake, C. *J. Alloys Compds.* **1995**, *225*, 334. Brink, J. M.; Rose, R. A.; Holz, R. C. *Inorg. Chem.* **1996**, *35*, 2878.
(63) Kemple, M. D.; Ray, B. D.; Lipkowitz, K. B.; Prendergast, F. G.; Rao, B. N. D. *J. Am. Chem. Soc.* **1988**, *110*, 8275.

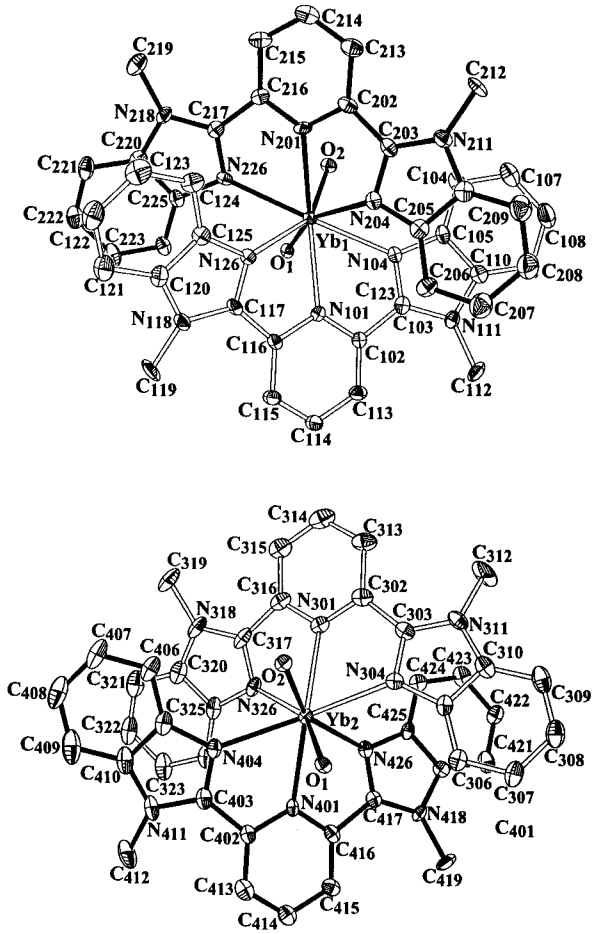

Figure 5. ORTEP drawing of $[Yb(OH)(L^1)_2]_2(ClO_4)_4(HClO_4)_{0.5}(CH_3CN)_{7.32}(L^1)_{0.5}$ (**1**) with the atom-numbering scheme.

Table 7. Selected Bond Lengths (Å) and Angles (deg) in $[Yb(OH)(L^1)_2]_2^{4+}$ (Standard Deviations in Parentheses)

Yb1−Yb2	3.6568(5)		
Yb1−O1	2.235(5)	Yb2−O1	2.233(4)
Yb1−O2	2.231(4)	Yb2−O2	2.231(5)
Yb1−N101	2.450(5)	Yb2−N301	2.509(5)
Yb1−N104	2.450(5)	Yb2−N304	2.424(5)
Yb1−N126	2.542(5)	Yb2−N326	2.567(5)
Yb1−N201	2.484(5)	Yb2−N401	2.479(5)
Yb1−N204	2.543(5)	Yb2−N404	2.457(5)
Yb1−N226	2.420(5)	Yb2−N426	2.543(5)
N104−Yb1−N101	65.3(2)	N304−Yb2−N301	65.1(2)
N101−Yb1−N126	63.5(2)	N301−Yb2−N326	62.7(2)
N204−Yb1−N201	63.2(2)	N426−Yb2−N401	63.6(2)
N201−Yb1−N226	64.9(2)	N404−Yb2−N401	65.4(2)
O1−Yb1−O2	70.0(2)	O1−Yb2−O2	70.1(2)
N104−Yb1−N204	69.9(2)	N304−Yb2−N426	69.9(2)
N204−Yb1−N126	82.6(2)	N426−Yb2−N326	84.2(2)
O2−Yb1−N201	76.5(2)	O1−Yb2−N401	78.3(2)
O1−Yb1−N226	83.4(2)	O2−Yb2−N404	83.8(2)
N226−Yb1−N126	69.5(2)	N326−Yb2−N404	69.8(2)
O1−Yb1−N101	78.7(2)	O2−Yb2−N301	77.0(2)
O2−Yb1−N104	84.4(2)	O1−Yb2−N304	83.3(2)

than the other (mean Yb−N difference: 0.11 Å) while differences smaller than 0.03 Å appear between the Yb−N(py) bond lengths. With respect to $[Lu(L^1)_2(MeOH)(H_2O)]^{3+}$,[27] the lengthening of the Ln−N bonds due to the larger ionic radius is greater for the benzimidazole N atoms (3 and 4%) than for the pyridine N atoms (2%). The effective Yb^{III} ionic radius defined according to Shannon[64] and calculated with $r_N = 1.46$ Å and $r_O = 1.31$ Å is 1.005 Å, close to the accepted value of 0.985 Å for 8-coordinate Yb^{III}.[5] The coordination polyhedra around the Yb^{III} ions are very similar and can be described as severely distorted cubes. N atoms from the central pyridines lie on two diametrically opposed vertices, and the two O atoms from the OH^- groups occupy the vertices of the same edge. The distortion arises from the constraint induced by the bonding of the three donor atoms of L^1 to Yb^{III}, as revealed by the mean N−Yb−N bite angle which is ≈64° for one ligand molecule as compared to 70.4° for an ideal cube. The two ligand strands are helically wrapped around each Yb^{III} ion, the Yb−Yb axis being the common axis of the two helical moieties, with torsion angles between the planar pyridine and benzimidazole groups ranging between about 17 and 25° as compared to 25° in $[Eu(L^1)_3]^{3+}$.[27] The dimer is further held together through stacking interactions between the almost parallel (7.0−7.2°) benzimidazole units of two ligand strands coordinated to different Yb^{III} ions (Figure F1, Supporting Information). In the unit cell, the dimeric cations are related by an inversion center, and they form long cylinders in the crystal, the empty spaces being filled by the anions and the uncoordinated ligand and solvent molecules (Figure F2, Supporting Information).

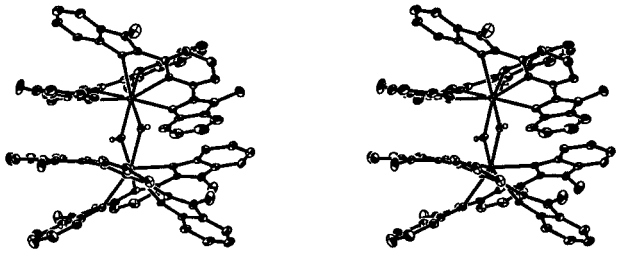

Figure 6. Stereoview of the cation $[Yb(OH)(L^1)_2]_2^{4+}$.

Stability of the Triple Helical Complexes with L^4. As $[Eu(L^1)_3]^{3+}$ complexes proved to be only faintly luminescent because the aromatic stacking interactions provide efficient deactivation paths for the excited $^5D_0$(Eu) level,[25−27] we have enhanced the antenna effect in these helicates by attaching 3,5-dimethoxybenzyl chromophores to the benzimidazole groups. The bulky aryl groups increase the solubility of both the ligand and its complexes, act as convenient NMR and MS probes, and indeed enhance the luminescent properties.[26,27] The thermodynamic stability of the $[Ln(L^4)_3]^{3+}$ species was investigated using the competitive potentiometric method with Ag^I in order to check whether the size-discriminating effect was retained or not.

Like L^1, L^4 self-assembles with Ag^I in acetonitrile to yield exclusively the D_2-symmetrical double-stranded helicate $[Ag_2(L^4)_2]^{2+}$. The dimeric structure is proven by the FAB-MS spectrum, which displays a sizable peak assigned to the perchlorate adduct $[Ag_2(L^4)_2(ClO_4)]^+$, and by the ^{1}H-NMR spectrum, very similar to the spectrum of $[Cu_2(L^4)_2]^{2+}$, except that the two doublets arising from the diastereotopic methylene protons (AB spin system) are broader for Ag^I, pointing to a more rapid exchange between the helical enantiomers.[50,51] The stability constant of the dimeric silver species, as determined by direct potentiometric titration in dry MeCN (25 °C, 0.1 M Et_4NClO_4, <10 ppm of H_2O), is $\log \beta_{22} = 11.3 \pm 0.2$, a value substantially lower than the one obtained with L^1.

The interaction between L^4 and Ln^{III} ions also proved to be weaker than that with L^1. The same model was used for interpreting the potentiometric data, but both $\log K_2$ and $\log K_3$ could be fitted in view of the reduced stability of the corresponding $[Ln(L^4)_n]^{3+}$ species ($n = 2, 3$). The 1:1 complexes, however, appeared to be as stable as with ligand L^1, and no reliable value could be extracted for $\log K_1$, the fit being insensitive to variation of this parameter within several orders

(64) Shannon, R. D. *Acta Crystallogr.* **1976**, *A32*, 751.

of magnitude, so that log K_1 was kept constant (>9) during the last iterations. Both log K_2 and log K_3 show little variation with Z, and they are respectively 2 and 4 orders of magnitude smaller than the same data for L^1. This effect is attributed to the conformational change of the tridentate units which occurs upon complexation (transoid−transoid in the free ligand → cisoid−cisoid in the complex).[28,29,31] Molecular mechanics suggests that bulky R^2 groups, as in L^4, produce strong steric interactions with H^5 in the cisoid−cisoid conformation, thus destabilizing the final complexes compared to those with L^1. On the other hand, the loss of the size-discriminating effect is assigned to the increased difficulty for L^4 to provide a tight coordination cavity around the Ln^{III} ions because of the presence of sterically demanding dimethoxybenzyl groups which are put close together by the wrapping process.[26]

Stability of the Triple Helical Complexes with L^8 and L^7. To overcome the difficulties encountered with ligand L^4, we have attached an electron-donating group to the central pyridine in L^8 to increase the strength of the interaction with Ln^{III} ions. The stability constants have been determined by the competitive potentiometric method with Ag^I. As usual, we have checked that $[Ag_2(L^8)_2]^{2+}$ is the only significant complex in solution upon titration of L^8 by Ag^I in solution (^{1}H-NMR, ES-MS). The ES-MS spectrum of a 2×10^{-4} M solution in MeCN essentially displays one intense peak (*m/z* 867.3) assigned to the dimeric species $[Ag_2(L^8)_2]^{2+}$ with very minor peaks corresponding to traces of 1:2 and 2:3 complexes. The 2:2 complex $[Ag_2(L^8)_2]^{2+}$ sustains decomposition in the gas phase under collision-induced dissociation to give $[Ag(L^8)]^+$ as previously reported for the Cu(I) analogue.[65] The stability constant of the dimeric silver species, as determined by direct potentiometric titration in dry MeCN (25 °C, 0.1 M Et_4NClO_4, ≈10 ppm of H_2O), is log β_{22} = 13.5 ± 0.1 (13.6 ± 0.1 in the presence of Ln^{III}), a value again comparable to that obtained with L^1. The potentiometric data for the $Ln^{III}/Ag^I/L^8$ systems have been satisfactorily fitted to the four equations (1) and (2). Due to its large value, log K_1 (>11) has been fixed while log K_2 could be refined for Tm and Yb but not for the other Ln's; in the latter cases it was fixed to a value >8. The general trend of log K_3 follows closely that obtained for $[Ln(L^1)_3]^{3+}$ (Table 2, Figure 2), especially for Sm−Yb. The triple-helical complexes with L^8 are slightly less stable than those with L^1 in the first part of the lanthanide series, but the size-discriminating effect is fully restored, $[Yb(L^8)_3]^{3+}$ being 10^3 times less stable than $[Gd(L^8)_3]^{3+}$, as observed with L^1.

The influence of an increased electron density on the formation of the mononuclear 1:3 complexes is confirmed with L^7: the introduction of an electron-attracting group, *p*-nitrophenyl, on the central pyridine ring leads to a substantially weaker interaction with Ln^{III} ions. No 1:3 complexes could be isolated or evidenced, and a spectrophotometric titration of the Eu^{III}/L^7 system yielded log $K_1 = 8.2 \pm 0.3$ and log $K_2 = 5.2 \pm 0.3$ (25 °C, 0.1 M Et_4NClO_4).

Discussion

The stability constants reported in Table 2 confirm that ligands L^i are efficient tridentate binding units for Ln^{III} ions, with overall stability in the range log $\beta_3 = 18-23$ for L^1, L^8 and log $\beta_3 \approx 17$ for L^4. This is in line with an earlier observation that neutral heterocyclic N atoms are among the best chelating atoms for Ln^{III} ions,[66,67] a fact confirmed by the large number of stable polyaza macrocyclic and Schiff base lanthanide complexes.[11,14] The stability of the $[Ln(L^i)_3]^{3+}$ complexes is however largely influenced by the substituents borne by the benzimidazole and central pyridine groups. The latter acts on the electron density of the pyridyl N atom, and stability differences up to $\Delta \log K_3 = 3$ occur between L^4 and L^8, while no 1:3 complexes form with L^7. Within the lanthanide series, a large size-discriminating effect is observed with L^1 and L^8, complexes with the heaviest Ln^{III} being 10^3-10^4 times less stable than those with the midrange Ln^{III} ions. The break in the stability versus $1/r_i$ curve appears for the same lanthanide ion, Gd^{III} for both L^1 and L^8, but other ligands are presently being synthesized with the aim of displacing the maximum of stability along the lanthanide series. The size-discriminating effect observed is large and compares in size with the selectivity achieved for heavy lanthanide ions by a water-soluble N_4O_3 tripodal amine phenol ligand: $\Delta \log \beta_2(Yb-Nd) = 5.5$.[68] On the other hand, it contrasts with the usually observed electrostatic trend leading to a continuous increase in stability with decreasing ionic radii,[58,68] the latter behavior being indeed observed for other series of semirigid tridentate ligands investigated in our laboratories, namely 2,6-pyridinedicarboxylic acid bis(ethylamide) and bis(ethyl ester).[61] The detailed structural characterization of $[Ln(L^1)_3]^{3+}$ sheds light on the origin of this remarkable size-discriminating effect. As demonstrated by paramagnetic NMR spectra, the closely packed triple-helical structure found for $[Eu(L^1)_3]^{3+}$ in the solid state[27] is retained in solution except for a slight straightening of the ligand along the C_3 axis. We thus conclude that the strong interstrand $\pi-\pi$ stacking interactions evidenced in the crystal structure still hold in solution. According to the accepted theory of $\pi-\pi$ interactions,[69] the interstrand separation in $[Eu(L^1)_3]^{3+}$ (3.1−3.3 Å)[27] is optimum and a contraction of the cavity to fit smaller Ln^{III} is expected to be difficult, leading to less stable complexes with the heavier Ln^{III} ions. We cannot completely rule out possible solvation effects associated with the increased affinity of small Ln^{III} ions for water.[5,23] However, the low water content of our solution (<50 ppm) and the minor effect of added water on the stability constants of $[Sm(L^1)_3]^{3+}$ ($\Delta \log K_3 \approx 0.2$) strongly suggest that these effects are not large enough to explain the observed drop in stability $\Delta \log K_3(Gd-Lu) \approx 3$. When bulky substituents are bound to the benzimidazole side arms, as in L^4, the wrapping of the strands in $[Ln(L^4)_3]^{3+}$ is severely hindered as observed in the crystal structure of $[Eu(L^5)_3]^{3+}$, where the strands are shifted to minimize the steric repulsion between the packed ethyl groups.[26] The resulting weaker interstrand π-stacking interactions give less stable triple-helical complexes $[Ln(L^4)_3]^{3+}$ and remove the size-discriminating effect. Interestingly, the latter can be restored by increasing the Ln−N(pyridine) interaction in $[Ln(L^8)_3]^{3+}$, which overcomes these destabilizing steric constraints.

Conclusion

Ligands L^{1-8} represent a library of rigid tridentate binding units possessing tunable electronic and structural properties which control the thermodynamic stability of the resulting triple-helical lanthanide building blocks $[Ln(L^i)_3]^{3+}$. Although the usual trend in Ln^{III} coordination chemistry with acyclic ligands is a smooth and uniform increase in stability with decreasing ionic radii,[58,68] the structural restrictions imposed by the aromatic

(65) Hopfgartner, G.; Piguet, C.; Henion, J. D.; Williams, A. F. *Helv. Chim. Acta* **1993**, *76*, 1759. Hopfgartner, G.; Piguet, C.; Henion, J. D. *J. Am. Soc. Mass Spectrom.* **1994**, *5*, 748.
(66) Thompson, L. C.; Shafer, B. L.; Edgar, J. A.; Mannila, K. D. *Adv. Chem. Ser.* **1967**, *71*, 169.
(67) Thompson, L. C. In *Handbook on the Physics and Chemistry of Rare Earths*; Gschneidner, K. A., Jr., Eyring, L., Eds.; North Holland: Amsterdam, 1979; pp 209−97.
(68) Caravan, P.; Hedlund, T.; Liu, S.; Sjoberg, S.; Orvig, C. *J. Am. Chem. Soc.* **1995**, *117*, 11230.
(69) Hunter, C. A.; Sanders, J. K. M. *J. Am. Chem. Soc.* **1990**, *112*, 5525. Hunter, C. A. *Angew. Chem., Int. Ed. Engl.* **1993**, *32*, 1584.

ligands L^i produce an inverted selectivity with a significant preference for the larger Ln^{III} ions and a maximum affinity for the midrange ions (Gd^{III}). Such a tunable selectivity is crucial for the design of self-assembled polymetallic systems since we have demonstrated that a small difference in binding affinity may result in highly selective processes leading to pure heterodinuclear assemblies such as $[LnM(L^i)_3]^{5+}$ ($i = 9, 10$; M = Zn, Fe).[28−33] In this context, the combination of a tridentate receptor predisposed[35] for the recognition of large Ln^{III} ions, such as L^i ($i = 1, 8$), with a tridentate ligand coded for small Ln^{III} ions in an unsymmetrical segmental ligand opens new perspectives for the preparation of pure heterodinuclear f−f complexes. This approach is currently being investigated in our laboratories.

Acknowledgment. We gratefully acknowledge C. Sager and M. V. Ferrel for collaborating on this project and C. Saint-Léger for her technical assistance. C.P. thanks the Werner Foundation for a fellowship. This work was supported by grants from the Swiss National Science Foundation.

Supporting Information Available: Tables S1−S3, listing contact and pseudocontact contributions and relaxation times, Tables S4−S7 giving atomic coordinates, equivalent isotropic and anisotropic displacement parameters, hydrogen coordinates, and least-squares plane data for $[Yb(OH)(L^1)_2]_2(ClO_4)_4(HClO_4)_{0.5}(CH_3CN)_{7.32}(L^1)_{0.5}$, and Figures F1−F2, displaying stacking interactions and the unit cell (22 pages). Ordering information is given on any current masthead page.

IC970693T